

Squeezing Marsquakes out of groundwater

Michael Manga¹, Guang Zhai¹, and Chi-Yuen Wang¹

¹University of California, Berkeley

November 22, 2022

Abstract

Pore pressure in aquifers confined below a cryosphere will increase as Mars cools and the cryosphere thickens. The increase in pore pressure decreases the effective stress and hence will promote seismicity. We calculate the rate of pore pressure change from cooling of the Martian interior and the modulation of pore pressure from solar and Phobos tides and barometric loading. Using the time-varying pressure and tidal stresses, we compute Coulomb stress changes and the expected seismicity rate from a rate-and-state friction model. Seismicity rate will vary by several 10s of percent to two orders of magnitude if the mean pore pressure is within 0.2 MPa and 0.01 MPa of lithostatic, respectively. Seismic events promoted by high pore pressure may be tremor-like. Documenting (or not) tidally-modulated shallow seismicity would provide evidence for (or against) water-filled confined aquifers, that pore pressure is high, and that the state of stress is close to failure — with implications for processes that can deliver of water to the Martian surface.

Squeezing Marsquakes out of groundwater

Michael Manga^{1,2}, Guang Zhai^{1,3}, and Chi-Yuen Wang¹

¹Department of Earth and Planetary Science, University of California, Berkeley, CA 94720, USA

²Center for Integrative Planetary Science, University of California, Berkeley, CA 94720, USA

³Berkeley Seismological Laboratory, University of California, Berkeley, CA 94720, USA

Key Points:

- Freezing aquifers become pressurized
- High pore pressure promotes seismicity
- Tides from the Sun and Phobos and barometric loading can modulate seismicity if pore pressure is high

Abstract

Pore pressure in aquifers confined below a cryosphere will increase as Mars cools and the cryosphere thickens. The increase in pore pressure decreases the effective stress and hence will promote seismicity. We calculate the rate of pore pressure change from cooling of the Martian interior and the modulation of pore pressure from solar and Phobos tides and barometric loading. Using the time-varying pressure and tidal stresses, we compute Coulomb stress changes and the expected seismicity rate from a rate-and-state friction model. Seismicity rate will vary by several 10s of percent to two orders of magnitude if the mean pore pressure is within 0.2 MPa and 0.01 MPa of lithostatic, respectively. Seismic events promoted by high pore pressure may be tremor-like. Documenting (or not) tidally-modulated shallow seismicity would provide evidence for (or against) water-filled confined aquifers, that pore pressure is high, and that the state of stress is close to failure - with implications for processes that can deliver of water to the Martian surface.

1 Introduction

Seismic signals on Mars are expected from meteorite impacts (e.g., Teanby, 2015) or may have a geodynamic origin from lithospheric stresses and ongoing mantle convection (e.g., Phillips, 1991; Golombek et al., 1992; Knapmeyer et al., 2006; Panning et al., 2017). Here we propose another internal mechanism to create marsquakes that is analogous to induced seismicity on Earth and may be modulated by tides.

Mars may host aquifers containing liquid water confined below a cryosphere (e.g., Clifford and Parker, 2001). As Mars cools, this cryosphere will thicken. If the pore space beneath the cryosphere is saturated with liquid water, the volume expansion from freezing will pressurize the remaining liquid in global or regional aquifers (e.g., Gaidos, 2001; Wang et al., 2006). As pore-pressure increases, critically-stressed faults are prone to slip and will thus generate Marsquakes. On Earth, if the pore-pressure changes are anthropogenic, the earthquakes are termed “induced” – induced seismicity is widespread where fluids are injected into the crust (Zoback and Gorelick, 2012; Ellsworth, 2013), especially from large volume injection of wastewater in Texas (e.g., Frohlich, 2012; Shirzaei et al., 2016), Oklahoma (e.g., Keranen et al., 2014) and Kansas (e.g., Schoenball and Ellsworth, 2017).

Pore pressures and crustal stresses are further modulated by solar, satellite and barometric tides. If faults are critically-stressed and close to failure, we might expect a tem-

poral modulation of seismicity. Tides trigger deep moonquakes (e.g., Lammlein, 1977; Lognonne and Johnson, 2015). Tidal modulation of seismicity has also been documented on Earth at all types of plate boundaries, including mid-ocean ridges (e.g., Tolstoy et al., 2002), along transform boundaries (e.g., vanderElst et al., 2016) and in the form of non-volcanic tremor in subduction zones (Rubinstein et al., 2008). Quakes caused by tides have been predicted for Europa (e.g., Hurford et al., 2019). Thus it is not unreasonable to expect that Marsquakes might also be influenced by tides, though tidal stresses will be smaller on Mars than on these other solar system bodies.

Here we compute the rate of pressure change in freezing aquifers and the modulation of that pressure from solar and Phobos tides and diurnal variations in barometric pressure. We can then compute Coulomb stress changes from tides. Using a rate-and-state friction model (Dieterich, 1994; Segall and Lu, 2015) we can predict the temporal modulation of seismicity induced in confined aquifers. We show that if background pore pressures are close to lithostatic – and hence also close to those needed to expel groundwater to the Martian surface – then there should be a tidal modulation of seismicity.

2 Pressurizing the cryosphere

Let b be the thickness of the frozen subsurface, with surface temperature T_0 and melting temperature T_m being the temperatures at the top and bottom of this layer, respectively. Thermal conductivity is k . A decreasing heat flow over time t , will increase b .

To compute db/dt we rely on the decrease of heat flow obtained from numerical simulations of thermal evolution that include cooling, declining radiogenic heat production, and mantle convection. For a range of interior models and properties, present day heat flow Q_0 is about 0.025 W/m^2 and is currently decreasing by about 0.0046 W/m^2 per Ga (Plesa et al., 2015). Parro et al. (2017) favor heat flows that are a bit lower, 0.014 to 0.025 W/m^2 , with an average of 0.019 W/m^2 . Uncertainties in these values are small (factor of two) compared to uncertainties in other parameters that influence seismicity rate changes.

Neglecting any heat production within the frozen cryosphere,

$$b = k \frac{(T_m - T_0)}{Q_0} \quad (1)$$

and hence

$$\frac{db}{dt} = -k \frac{(T_m - T_0)}{Q_0^2} \frac{dQ_0}{dt}. \quad (2)$$

Assuming a constant $k = 1.5$ W/mK (Hartlieb et al., 2016), $T_0 = 220$ K and $T_m = 273$ K, then $b = 3180$ m and $db/dt = 1.85 \times 10^{-14}$ m/s (equivalent to 585 m/Ga). The exact depth of the cryosphere at a given location depends on the local heat flow, thermal conductivity of the crust, the salinity (composition) of the pore water (Clifford et al., 2010; Sori and Bramson, 2019), and whether or not the addition of ice to the base of the cryosphere is supply- or heat-limited (e.g., Weiss and Head, 2017). T_m could be several degrees lower than the assumed value if freezing leaves behind sufficient salt in the aquifer (Mikucki et al., 2015). The thermal conductivity of dry, shallow regolith may be much lower, and is very sensitive to the fraction of pore space filled with ice (e.g., Siegler et al., 2012).

To compute the change in pore pressure we first need to compute the change in the amount of fluid/unit volume df that arises from the 9% expansion of liquid water as it freezes. We assume that porosity ϕ decreases exponentially with depth with scale length δ ,

$$\phi(z) = \phi_0 e^{-z/\delta}. \quad (3)$$

The total volume of liquid water/unit area V below the cryosphere is thus

$$V = \phi_0 \int_b^\infty e^{-z/\delta} dz = \phi_0 \delta e^{-b/\delta}. \quad (4)$$

The rate that liquid water is added to V from the 9% expansion of liquid water as it freezes is $0.09\phi_0 e^{-b/\delta} db/dt$. The increment of fluid content f thus varies over time

$$\frac{df}{dt} = \frac{0.09\phi_0 e^{-b/\delta}}{V} \frac{db}{dt}. \quad (5)$$

Choosing $\delta = 3$ km (e.g., Clifford, 1993; Hanna and Phillips, 2005) and $\phi_0 = 0.4$ (Lewis et al., 2019), we obtain $df/dt = 5.6 \times 10^{-19}$ s $^{-1}$.

The corresponding change in pore pressure p is computed using a linear poroelastic model (e.g., Wang, 2000)

$$\frac{dp}{dt} = \frac{K_u B}{\alpha} \frac{df}{dt}, \quad (6)$$

where K_u is the undrained bulk modulus, α is the Biot-Willis coefficient, B is Skempton's coefficient, df originates from the freezing of the aquifer, and we assume this freezing is sufficiently slow that hydraulic head is uniform in the aquifer. There is much uncertainty in the relevant poroelastic properties. Here we adopt those summarized by Wang (2000) for Hanford basalt: $K_u = 45.4$ GPa, $\alpha = 0.23$ and $B = 0.12$. This leads to $dp/dt = 1.33 \times 10^{-8}$ Pa/s.

There are considerable uncertainties in Q_0 , T_m , k , poroelastic constants, and likely lateral heterogeneities in the region (Golombek et al., 2018), that cumulatively might lead to an order of magnitude uncertainty in the secular stressing rate dp/dt . As we will see, uncertainties in dp/dt have a small effect on the tidal modulation of seismicity. But b will affect the depth at which the seismicity would occur, and hence documenting the depth of any tidally induced seismicity should better constrain some of the poorly constrained properties of crust such as Q_0 , T_m and k .

3 Tidal stresses and pressure modulation

We consider three sources of periodic deformation: changes in the gravitational potential from the Sun and Phobos, and diurnal barometric loading from atmospheric thermal tides. The geometry and equations for the time-varying strain tensor are given in the supplement. We use degree 2 Love numbers $h_2 = 0.29$ (Genova et al., 2016; Konopliv et al., 2016) and $l_2 = 0.038$ (Sohl and Spohn, 1997), and a shear modulus of 20 GPa. We assume pure elastic deformation and neglect the lag in tidal deformation, about 0.3 degrees for Phobos tides (e.g., Bills et al., 2005; Jacobson and Lainey, 2014).

The induced pore pressure p is

$$p = -K_u B \epsilon + B \bar{\sigma}, \quad (7)$$

where ϵ is the volumetric strain from tides (positive for expansion) and $\bar{\sigma}$ is the volumetric stress responding to the diurnal barometric loading (positive for compression). In the supplement we describe the procedures for computing stresses and strains.

The Coulomb stress σ_c is computed from the tide-induced shear stress τ and normal stress σ_n (positive for clamping) by

$$\sigma_c = \tau - \mu(\sigma_n - \alpha p). \quad (8)$$

The friction coefficient $\mu = 0.6$ (Byerlee, 1978).

Figure 2 shows the evolution of pore pressure and Coulomb stress at the Mars In-Sight lander location (4.5°N 135.9°E) for a vertical fault with a range of strikes.

The magnitudes of the tidal stresses and pore pressure changes are small (of order 10^2 Pa). However, the tidal stressing rate is several orders of magnitude larger than the secular rate of pressurization from freezing aquifers. If the shallow crust is critically-stressed by the long-term thermal contraction (e.g., Knapmeyer et al., 2006), mantle convection (Plesa et al., 2016) or freezing of aquifers (section 2), then faults near failure may

be ubiquitous and the tidal stresses and pore pressures may trigger earthquakes on critically-stressed faults. The relatively large magnitude of tidal forcing may control the timing of seismicity.

4 Predicting seismicity rate on Mars

To predict seismic activity on Mars, we use a laboratory-derived rate-and-state earthquake nucleation model (Dieterich, 1994). This model simulates the temporal evolution of seismicity rate due to a change of Coulomb failure stress and assumes that fault systems are critically-stressed. A simplified version of the nucleation model (Segall and Lu, 2015) relates the history of relative seismicity rate R (seismicity rate relative to background seismicity rate) to the history of Coulomb stressing rate

$$\frac{dR}{dt} = \frac{R}{t_a} \left(\frac{\dot{\sigma}_c}{\dot{\tau}_0} - R \right) \quad (9)$$

where $\dot{\tau}_0$ is the background stressing rate from Mars' secular cryosphere cooling, which is the lower bound and may be as much as two orders of magnitudes larger, as summarized in Panning et al. (2017); $t_a = A\sigma_0/\dot{\tau}_0$ is the characteristic relaxation time; A is a constitutive parameter in the rate-and-state friction law (Dieterich, 1994); σ_0 is the background effective normal stress that depends on the absolute pore fluid pressure in the aquifers. The Coulomb stressing rate $\dot{\sigma}_c$ is calculated from equation (8) by superimposing the tidal and barometric loading induced pore pressure history p and the Coulomb stress without pore pressure (Figure 2). We use the value of $A = 0.003$ from Segall and Lu (2015) and highlight that its value and uncertainty are unknown for Mars. Values and uncertainties in A , σ_0 and $\dot{\tau}_0$ affect t_a hence we explore a range of t_a .

Using the stressing history (Figure 2), we can predict the temporal evolution of seismicity rate on Mars by integrating equation (9). Figure 3 shows that background effective normal stress σ_0 dominates the predicted seismicity rate changes from tidal and barometric effects. Parameters that affect b and db/dt and hence the background stressing rate have a relatively small effect because they are always much smaller than those produced by tides unless the effective normal stress is low. If the background normal stress is high, the fault system would be relatively stable to small stress fluctuations, making Marsquakes difficult to nucleate (Figure 3 top row). However, if the pore fluid pressure is close to lithostatic pressure such that the effective normal stress would be small, the fault system is sensitive to small stress fluctuations and the relative seismicity rate can approach 10^3 (Figure 3 bottom row). The nonlinearity of rate-and-state friction further

influences the seismicity rate as the effective normal stress becomes small. The increase in the number of Marsquakes can also elevate Marsquake magnitude by more than 2 orders following the Gutenberg-Richter earthquake magnitude-frequency relationship.

Figure 3 shows how the seismicity rate R is expected to vary. We do not, at the present time, convert the seismicity rate to a prediction of Mars' total marsquake magnitude-time distribution, which could be compared with data from InSight. To do so requires three additional steps, in addition to knowing the background seismicity rate: 1) integrating R over the surface of Mars, 2) accounting for attenuation and scattering in the shallow crust, and 3) modeling the noise environment produced from thermal effects and wind which will vary throughout the Martian day and over seasons. InSight should provide much of the data needed to do this calculation.

Since Mars' orbit has large eccentricity that causes the gravitational attraction of the Sun to change by a factor of 1.74 per orbit, we expect a further modulation of Marsquakes throughout the year (Supplementary Figure S3). Identifying variations in seismicity from semi-diurnal to annual timescales may help distinguish the origin of the stress connected to Marsquakes and hence provide an opportunity to identify groundwater-induced seismicity.

5 Discussion

The physics used to compute whether tidal stresses and freezing aquifers influence seismicity are similar to those used to forecast induced seismicity on Earth (e.g., Zhai and Shirzaei, 2018; Goebel et al., 2018). There are, however, many poroelastic and aquifer properties (K_u , B , α , ϕ_0 , δ) that are not observationally-constrained on Mars, and statistical properties of seismicity that enter the rate-and-state friction model (A , $\dot{\tau}_0$) are not known. As a consequence, there are corresponding uncertainties in the mean seismicity rate and its modulation. The parameter, however, that is most uncertain and has the largest effect on the magnitude of R is σ_0 , the background effective normal stress (that depends on the mean pore fluid pressure in the aquifers) as it leads to a rapid change in seismicity rate as pore pressure approaches lithostatic. Uncertainties in the parameters that control b primarily affect the depth at which any tidally modulated seismicity would occur. Thus, the general conclusion that tidal modulation is expected if pore pressure is close to lithostatic should be a robust conclusion.

Identifying any tidal modulation of shallow seismicity could then be used to better constrain properties of the Martian crust and any aquifers it hosts, at least in the vicinity of the InSight landing site (Golombek et al., 2018) – seismicity enabled by high pore pressure is expected to occur near the base of the cryosphere. Tidally induced seismicity might also be tremor-like, similar to non-volcanic tremor on Earth that is often attributed to high pore pressures (e.g., Beroza and Ide, 2011). The first reported Marsquake on sol 128 (reported by the InSight team on April 23, 2019) does in fact look tremor-like, but this type of waveform could also be the result of multiple scattering in the crust.

We have drawn an analogy of the hypothesized tidally-modulated seismicity to induced seismicity on Earth because high fluid pressures promote slip and pressure variations modify the timing of seismic events. There is, however, a quantitative difference because the pore pressure changes from tidally-induced strains are relatively small compared to the shear stresses – the relative magnitude of pressure and shear stress changes from tides are small compared to the equivalent from fluid injection. Tidal modulation of seismicity does not necessitate high fluid pressure change - deep moonquakes provide a counter example – but does require small effective normal stresses.

The outflow channels on Mars are usually attributed to the catastrophic release of groundwater from the Martian subsurface (e.g., Carr, 1979). Discharge from present-day aquifers has also been suggested as a mechanism to form smaller features such as gullies and recurring slope linea (e.g., Malin and Edgett, 2000; Mellon and Phillips, 2001; Heldmann et al., 2005; Stillman et al., 2014), possibly enabled because high salinity can decrease the depth at which aquifers remain stable (Ohja et al., 2015; Stillman et al., 2016). Yet the source of the water and the mechanism by which the water is released remain uncertain (e.g., Clifford and Parker, 2001; Wang et al., 2005; Hanna and Phillips, 2005, 2006; Grimm et al., 2017). Freezing of aquifers may allow pore pressure to approach lithostatic pressure at the base of the cryosphere and hence to rupture the cryosphere, leading to groundwater discharge on the Martian surface (e.g., Gaidos, 2001; Wang et al., 2006). It remains uncertain, however, whether pressurization of Martian aquifers by gradual freezing can create sufficiently high enough pore pressure to rupture the cryosphere (Hanna and Phillips, 2005), though water loss has been low enough that groundwater should at least persist globally (Grimm et al., 2017). Pressure in aquifers confined by a cryosphere may also be elevated if they are recharged at higher elevation (e.g., Harrison and Grimm, 2004; Andrews-Hanna and Lewis, 2011).

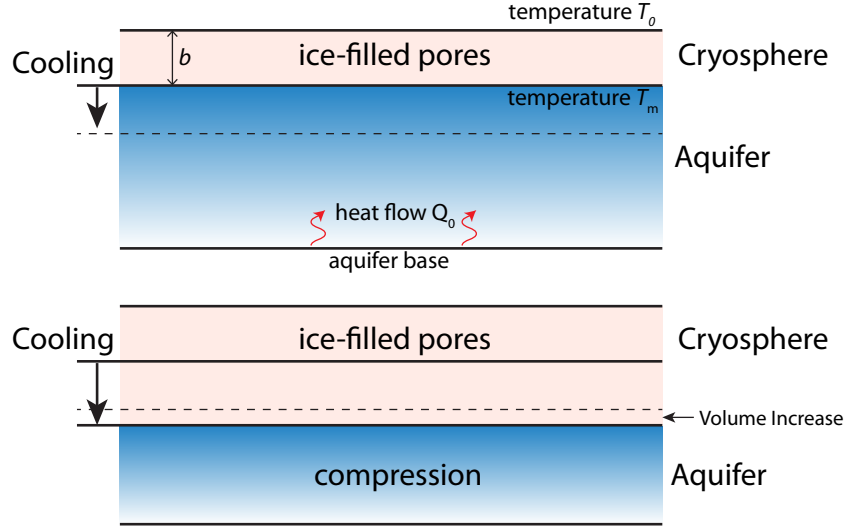


Figure 1. As Mars cools, the boundary between frozen ground and liquid water in aquifers moves downward. The volume expansion upon freezing will compress the remaining liquid water and increase pore pressure in aquifers.

The ideas and processes considered here for Mars may not be confined to rocky planets with groundwater systems (Earth and Mars). Fracturing by overpressure that develops in water confined by a freezing ice shell has also been invoked for icy satellites, both for water confined in a global ocean (e.g., Manga and Wang, 2007) or possibly in isolated pockets of water (e.g., Fagents, 2003; Manga and Michaut, 2017).

6 Summary

Shallow tidally-modulated seismicity, if documented by InSight or the accelerometer on Curiosity (Lewis et al., 2019), would provide evidence of liquid-filled confined aquifers with near-lithostatic pore pressure and a state of stress close to that required for failure. Conversely, an absence of tidal modulation of seismicity implies low pore pressure, with implications for the properties of Martian groundwater systems and the processes that allow liquid water to be delivered to the Martian surface. Constraining the depth of Mars' cryosphere and whether it is underlain by liquid water are critical to understanding Mars' past and present near-surface water budget (Carr and Head, 2015). The presence or absence of induced seismicity provides an opportunity to better constrain the state and amount of subsurface water.

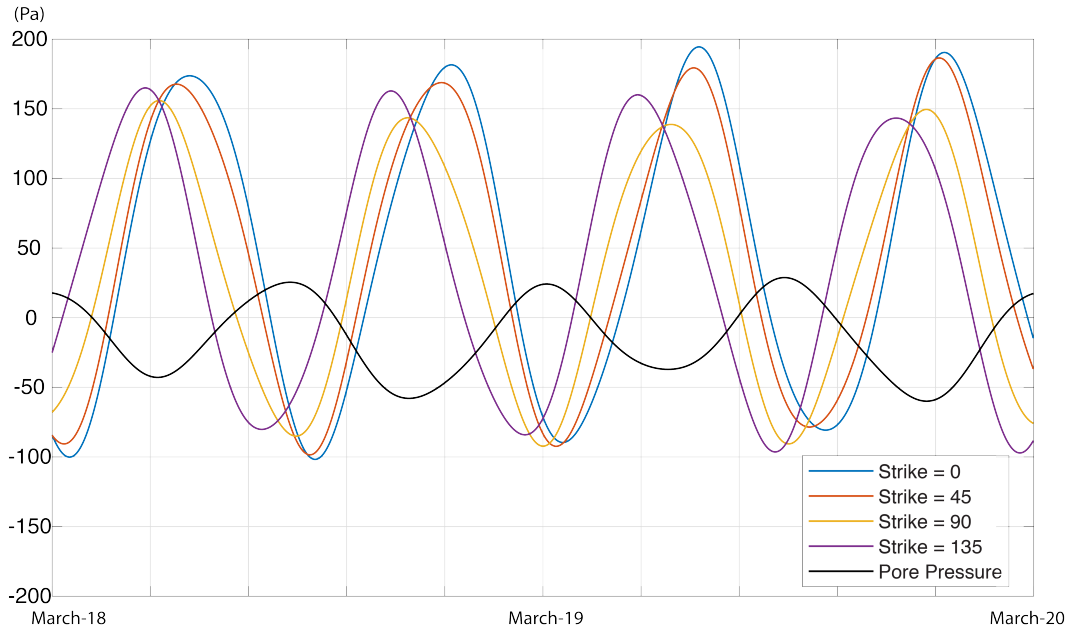


Figure 2. Time series of Coulomb stress change for different fault azimuths (vertical faults) and pore pressure change due to the combined effect of solar and Phobos tides and barometric loading. We assume the location of the InSight lander. Dates are Earth dates in 2019.

Acknowledgments

MM supported by NASA 80NSSC19K0545, CW by NSF 1463997 and GZ by DOE DE-SC0019307. We thank the entire InSight team for their persistence and dedication to a most remarkable geophysical achievement, and the editor and two reviewers for constructive and thoughtful comments. No data was is presented in this paper. Curves in figures 2 and 3 are produced by solving the equations in the paper.

References cited

- Andrews-Hanna, J. C., and Lewis, K. W. (2011). Early Mars hydrology: 2. Hydrological evolution in the Noachian and Hesperian epochs. *Journal of Geophysical Research: Planets*, 116(E2). doi.org/10.1029/2010JE003709
- Beroza, G. C., and Ide, S. (2011). Slow earthquakes and nonvolcanic tremor. *Annual Reviews of Earth and Planetary Sciences*, 39, 271296, doi:10.1146/annurev-earth-040809-152531.
- Bills, B.G., Neumann, G.A., Smith, D.E., and Zuber, M.T. (2005). Improved estimate of tidal dissipation within Mars from MOLA observations of the shadow of Phobos. *Journal of Geophysical Research*, 110, 115.

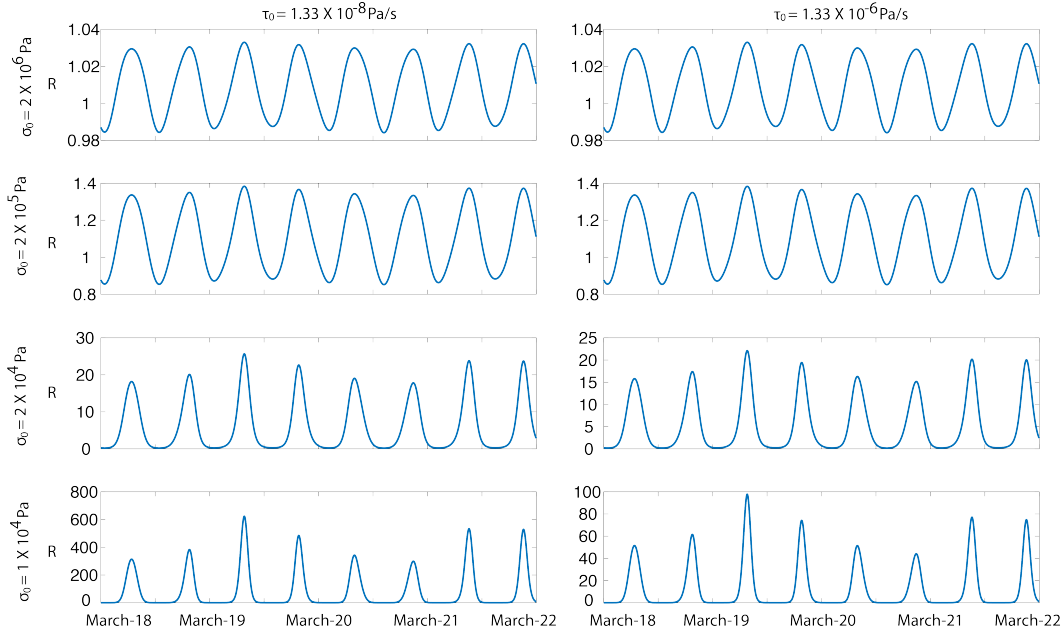


Figure 3. The simulated time series of relative seismicity rate R due to imparted stresses and pore pressure changes assuming $A = 0.003$ (Segall and Lu, 2015) for different scenarios of background effective normal stress σ_0 and background stressing rate $\dot{\tau}_0$ (lower limit is the stressing rate from freezing the cryosphere and the larger value is 100 times larger). We consider σ_0 as large as 2 MPa. We consider a lower value of σ_0 by choosing a lower bound of 0.5% of largest σ_0 . Dates are Earth dates in 2019.

- 264 Byerlee, J. (1978). Friction of Rocks. *Pure and Applied Geophysics*, 116, 615-626.
- 265 Carr, M.H. (1979). Formation of Martian flood features by release of water from con-
266 fined aquifers. *Journal of Geophysical Research*, 87, 6781-6790.
- 267 Carr, M.H., and Head, J.W. (2015). Martian surface/nearsurface water inventory: Sources,
268 sinks, and changes with time. *Geophysical Research Letters*, 42(3), 726-732.
- 269 Clifford, S.M. (1993). A model for the hydrologic and climatic behavior of water on Mars.
270 *Journal of Geophysical Research*, 98, 10,973-11,016.
- 271 Clifford, S. M., and Parker, T.J. (2001). The evolution of the Martian hydrosphere: Im-
272 plications for the fate of a primordial ocean and the current state of the northern plains.
273 *Icarus*, 154, 4079.
- 274 Clifford, S. M., Lasue, J., Heggy, E., Boisson, J., McGovern, P., and Max, M. D. (2010).
275 Depth of the Martian cryosphere: Revised estimates and implications for the existence
276 and detection of subpermafrost groundwater. *Journal of Geophysical Research: Plan-
277 ets*, 115(E7). doi:10.1029/2009JE003462
- 278 Dieterich, J. (1994). A constitutive law for rate of earthquake production and its appli-
279 cation to earthquake clustering. *Journal of Geophysical Research*, 99(B2), 2601-2618.
- 280 Ellsworth, W. L. (2013). Injection-induced earthquakes. *Science*, 341(6142). doi.org/10.1126/science.1225942.
- 281 Fagents, S.A. (2003). Considerations for effusive cryovolcanism on Europa: The post-
282 Galileo perspective. *Journal of Geophysical Research*, 108, 5139, doi:10.1029/2003JE002128.
- 283 Frohlich, C. (2012). Two-year survey comparing earthquake activity and injection-well
284 locations in the Barnett Shale, Texas. *Proceedings of the National Academy of Sciences*,
285 109(35), 13934-13938.
- 286 Gaidos, E.J. (2001). Cryovolcanism and the recent flow of liquid water on Mars. *Icarus*,
287 153(1), 218-223.
- 288 Genova, A., Goossens, S., Lemoine, F.G., Mazarico, E., Neumann, G.A., Smith, D., and
289 Zuber, M.T. (2016). Seasonal and static gravity field of Mars from MGS, Mars Odyssey
290 and MRO radio science. *Icarus*, 272, 228-245. doi:10.1016/j.icarus.2016.02.050.
- 291 Goebel, T.H., and Brodsky, E.E. (2018). The spatial footprint of injection wells in a global
292 compilation of induced earthquake sequences. *Science*, 361(6405), 899-904.
- 293 Golombek, M., Banerdt, W., Tanaka, K., and Tralli, D. (1992). A prediction of Mars seis-
294 micity from surface faulting. *Science*, 258, 979-981.
- 295 Golombek, M., et al. (2018). Geology and Physical Properties Investigations by the In-
296 Sight Lander. *Space Science Reviews*, 214, 84, doi.org/10.1007/s11214-018-0512-7.

- 297 Grimm, R. E., Harrison, K. P., Stillman, D. E., and Kirchoff, M. R. (2017). On the sec-
298 ular retention of ground water and ice on Mars. *Journal of Geophysical Research: Plan-*
299 *ets*, *122*(1), 94-109.
- 300 Hanna, J. C., and Phillips, R.J. (2005). Hydrological modeling of the Martian crust with
301 application to the pressurization of aquifers. *Journal of Geophysical Research*, *110*, E01004,
302 doi:10.1029/2004JE002330.
- 303 Hanna, J. C., and Phillips, R.J. (2006). Tectonic pressurization of aquifers in the for-
304 mation of Mangala and Athabasca Valles, Mars. *Journal of Geophysical Research*, *111*,
305 E03003, doi:10.1029/2005JE002546.
- 306 Harrison, K.P., and Grimm, R.E. (2004). Tharsis recharge: A source of groundwater for
307 Martian outflow channels. *Geophysical Research Letters*, *31*(14). doi.org/10.1029/2004GL020502
- 308 Hartlieb, P., M. Toifl, F. Kuchar, R. Meisels and T. Antretter (2016). Thermo-physical
309 properties of selected hard rocks and their relation to microwave-assisted comminution.
310 *Minerals Engineering*, *91*, 34-41.
- 311 Heldmann, J. L., Toon, O. B., Pollard, W. H., Mellon, M. T., Pitlick, J., McKay, C. P.,
312 and Andersen, D. T. (2005). Formation of Martian gullies by the action of liquid wa-
313 ter flowing under current Martian environmental conditions. *Journal of Geophysical Re-*
314 *search: Planets*, *110*(E5). doi.org/10.1029/2004JE002261
- 315 Hurford, T.A., Henning, W.G., Maguire, R., Lekic, V., Schmerr, N., Panning, M., Bray,
316 V.J., Manga, M., Kattenhorn, S.A., Quick, L.C. and Rhoden, A.R. (2018). Seismicity
317 on Tidally Active Solid-Surface Worlds. arXiv preprint arXiv:1811.06536.
- 318 Jacobson, R.A., and Rainey, V. (2014). Martian satellite orbits and ephemerides. *Plan-*
319 *etary and Space Science*, *102*, 35-44.
- 320 Keranen, K., Weingarten, M., Abers, G., Bekins, B., and Ge, S. (2014). Sharp increase
321 in central Oklahoma seismicity since 2008 induced by massive wastewater injection. *Sci-*
322 *ence*, *345*(6195), 448451.
- 323 Knapmeyer, M., Oberst, J., Hauber, E., Wahlsch, M., Deuchler, C., and Wagner, R. (2006).
324 Working models for spatial distribution and level of Mars seismicity. *Journal of Geophys-*
325 *ical Research*, *111*(E11), doi:10.1029/2006JE002708.
- 326 Konopliv, A.S, Park, R.S., and Folkner, W.M. (2016). An improved JPL Mars gravity
327 field and orientation from Mars orbiter and lander tracking data. *Icarus*, *274*, 253260.
328 doi:10.1016/j.icarus.2016.02.052.

- 329 Lammlein, D. R. (1977). Lunar seismicity and tectonics. *Physics of the Earth and Plan-*
 330 *etary Interiors*, 14(3), 224-273.
- 331 Lewis, K.W., Peters, S., Gonter, K., Morrison, S., Schmerr, N., Vasavada, A.R., and Gabriel,
 332 T. (2019). A surface gravity traverse on Mars indicates low bedrock density at Gale crater.
 333 *Science*, 363, 535-537.
- 334 Lognonne, P., and Johnson, C.L. (2015). Planetary seismology, in *Treatise on Geophysics*,
 335 vol. 10, ed. by G. Schubert 2nd edition, Elsevier, Oxford, pp. 65120.
- 336 Malin, M. C., and Edgett, K. S. (2000). Evidence for recent groundwater seepage and
 337 surface runoff on Mars. *Science*, 288(5475), 2330-2335.
- 338 Manga, M., and Michaut, C. (2017). Formation of lenticulae on Europa by saucer-shaped
 339 sills. *Icarus*, 286, 261-269. dx.doi.org/10.1016/j.icarus.2016.1009.
- 340 Manga, M., and Wang, C.-Y. (2007). Pressurized oceans and the eruption of liquid wa-
 341 ter on Europa and Enceladus. *Geophysical Research Letters*, 34, L07202, 10.1029/2007GL029297.
- 342 Mellon, M. T., and Phillips, R. J. (2001). Recent gullies on Mars and the source of liq-
 343 uid water. *Journal of Geophysical Research: Planets*, 106(E10), 23165-23179.
- 344 Mikucki, J. A., et al. (2015). Deep groundwater and potential subsurface habitats be-
 345 neath an Antarctic dry valley. *Nature communications*, 6, 6831. doi:10.1038/ncomms7831.
- 346 Ojha, L., Wilhelm, M. B., Murchie, S. L., McEwen, A. S., Wray, J. J., Hanley, J., et al.
 347 (2015). Spectral evidence for hydrated salts in recurring slope lineae on Mars. *Nature*
 348 *Geoscience*, 8(11), 829-832.
- 349 Panning, M. P., Lognonn, P., Banerdt, W. B., Garcia, R., Golombek, M., Kedar, S., et
 350 al. (2017). Planned products of the Mars structure service for the InSight mission to Mars.
 351 *Space Science Reviews*, 211(1-4), 611-650.
- 352 Parro, L. M., Jimnez-Daz, A., Mansilla, F., and Ruiz, J. (2017). Present-day heat flow
 353 model of Mars. *Scientific Reports*, 7, doi 10.1038/srep45629
- 354 Phillips, R. (1991). Expected rate of marsquakes, in Scientific Rationale and Requirements
 355 for a Global Seismic Network on Mars, pp. 3538. *LPI Tech. Rept.*, 91-02, Lunar and Plan-
 356 etary Inst., Houston.
- 357 Plesa, A. C., Tosi, N., Grott, M., and Breuer, D. (2015). Thermal evolution and Urey
 358 ratio of Mars. *Journal of Geophysical Research: Planets*, 120(5), 995-1010.
- 359 Plesa, A. C., Grott, M., Tosi, N., Breuer, D., Spohn, T., and Wieczorek, M. A. (2016).
 360 How large are presentday heat flux variations across the surface of Mars? *Journal of Geo-*
 361 *physical Research: Planets*, 121(12), 2386-2403.

362 Rubinstein, J. L., La Rocca, M., Vidale, J. E., Creager, K. C., and Wech, A. G. (2008).
 363 Tidal modulation of nonvolcanic tremor. *Science*, *319*(5860), 186-189.

364 Schoenball, M., and Ellsworth, W. L. (2017). A systematic assessment of the spatiotem-
 365 poral evolution of fault activation through induced seismicity in Oklahoma and south-
 366 ern Kansas. *Journal of Geophysical Research: Solid Earth*, *122*(12). doi.org/10.1002/2017JB014850

367 Segall, P., and Lu, S. (2015). Injection-induced seismicity: Poroelastic and earthquake
 368 nucleation effects. *Journal of Geophysical Research: Solid Earth*, *120*, 50825103. doi.org/10.1002/2015JB012060.

369 Shirzaei, M., Ellsworth, W. L., Tiampo, K. F., Gonzalez, P. J., and Manga, M. (2016).
 370 Surface uplift and time-dependent seismic hazard due to fluid injection in eastern Texas.
 371 *Science*, *353*(6306), 14161419. doi.org/10.1126/science.aag0262.

372 Siegler, M., Aharonson, O., Carey, E., Choukroun, M., Hudson, T., Schorghofer, N., and
 373 Xu, S. (2012). Measurements of thermal properties of icy Mars regolith analogs. *Jour-
 374 nal of Geophysical Research: Planets*, *117*, E03001, doi:10.1029/2011JE003938.

375 Sohl, F. and Spohn, T. (1997). The interior structure of Mars: Implications from SNC
 376 meteorites. *Journal of Geophysical Research*, *102*, 16131635.

377 Sori, M.M. and Bramson, A.M. (2019). Water on Mars, with a grain of salt: Local heat
 378 anomalies are required for basal melting of ice at the South Pole today. *Geophysical Re-
 379 search Letters*, *46*(3), 10.1029/2018GL080985.

380 Stillman, D. E., Michaels, T.I., Grimm, R.E., and Harrison, K.P. (2014). New observa-
 381 tions of Martian southern midlatitude recurring slope lineae (RSL) imply formation by
 382 freshwater subsurface flows. *Icarus*, *233*, 328341, doi:10.1016/j.icarus.2014.01.017.

383 Stillman, D. E., Michaels, T.I., Grimm, R.E., and Hanley, J. (2016). Observations and
 384 modeling of northern midlatitude recurring slope lineae (RSL) suggest recharge by a present-
 385 day Martian briny aquifer. *Icarus*, doi:10.1016/j.icarus.2015.10.007.

386 Teanby, N.A. (2015). Predicted detection rates of regional-scale meteorite impacts on
 387 Mars with the InSight shortperiod seismometer. *Icarus*, *256*, 4962.

388 Tolstoy, M., Vernon, F. L., Orcutt, J. A., and Wyatt, F. K. (2002). Breathing of the seafloor:
 389 Tidal correlations of seismicity at Axial volcano. *Geology*, *30*(6), 503-506.

390 van der Elst, N. J., Delorey, A. A., Shelly, D. R., and Johnson, P. A. (2016). Fortnightly
 391 modulation of San Andreas tremor and low-frequency earthquakes. *Proceedings of the
 392 National Academy of Sciences*, *113*(31), 8601-8605.

393 Wang, H. (2000). Theory of Linear Poroelasticity With Applications to Geomechanics
 394 and Hydrogeology. Princeton Univ. Press, Princeton, N. J.

- 395 Wang, C.-Y., Manga, M., and Wong, A. (2005). Floods on Mars released from ground-
396 water by impact. *Icarus*, *175*, 551-555.
- 397 Wang, C. Y., Manga, M., and Hanna, J. C. (2006). Can freezing cause floods on Mars?
398 *Geophysical Research Letters*, *33*(20). doi.org/10.1029/2006GL027471
- 399 Weiss, D. K., and Head, J. W. (2017). Evidence for stabilization of the ice-cemented cryosphere
400 in earlier Martian history: Implications for the current abundance of groundwater at depth
401 on Mars. *Icarus*, *288*, 120-147.
- 402 Zhai, G., and Shirzaei, M. (2018). Fluid injection and time-dependent seismic hazard
403 in the Barnett Shale, Texas. *Geophysical Research Letters*, *45*, 4743-4753. doi.org/10.1029/2018GL077696.
- 404 Zoback, M. D., and Gorelick, S. M. (2012). Earthquake triggering and large-scale geo-
405 logic storage of carbon dioxide. *Proceedings of the National Academy of Sciences*, *109*(26),
406 10164-10168.